Global Change Biology Communications

WILEY

Global Change Biology Communications
BIOLOGY FOR A RAPIDLY CHANGING WORLD

RESEARCH ARTICLE OPEN ACCESS

Climate Controls on Carbon Dioxide Fluxes in a High-Elevation Grassland

Silvio Marta[1] | Marta Magnani[2,3] | Gianna Vivaldo[1,3] | Andrea Mainetti[4] | Ilaria Baneschi[1,3] | Alice Baronetti[1] | Simona Gennaro[1] | Mariasilvia Giamberini[1] | Simone Ravetto Enri[5] | Michele Lonati[5] | Brunella Raco[1] | Antonello Provenzale[2,3,6]

[1]Institute of Geosciences and Earth Resources, National Research Council, Pisa, Italy | [2]Institute of Geosciences and Earth Resources, National Research Council, Torino, Italy | [3]National Biodiversity Future Centre, Palermo, Italy | [4]Biodiversity Service and Scientific Research, Gran Paradiso National Park, Cogne, Italy | [5]Department of Agriculture, Forest and Food Sciences (DISAFA), University of Torino, Grugliasco, Italy | [6]CIMA Research Foundation, Savona, Italy

Correspondence: Silvio Marta (silvio.marta@cnr.it)

Received: 13 November 2025 | **Revised:** 5 March 2026 | **Accepted:** 23 March 2026

Keywords: Alpine ecosystems | climate change | ecosystem functioning | ecosystem respiration | flux chambers | gross primary productivity | growing degree days | remote sensing | snow cover dynamics

ABSTRACT

Climate change significantly influences natural and semi-natural ecosystems at global scale. This impact is further amplified in alpine environments, owing to a set of climate feedback mechanisms (i.e., elevation-dependent warming). Due to the short snow-free season and the consequent adaptation of alpine plants to fast growth, high-elevation grasslands mainly act as carbon sinks during the vegetative season, with primary productivity usually exceeding ecosystem respiration. We combined timeseries of field data (CO_2 fluxes and environmental variables), with weather, vegetation and remotely-sensed land-cover data from the Nivolet area (Gran Paradiso National Park, western Italian Alps), to identify the factors controlling diurnal ecosystem respiration and primary productivity in such environments. We found that growing-degree-days-since-snowmelt (GDD_0—a measure of cumulative heat available for plant growth since the snow has melted) exerted a strong control on both respiration and primary productivity. The effect of GDD_0 on productivity is both indirect, mediated by the seasonal trend in greening (proxied by vegetation indices), and direct, possibly reflecting the importance of cumulated heat on vegetation height. While greening had limited effect on respiration, GDD_0 had a strong effect, supporting the view that ecosystem respiration was mainly temperature-related and microbial-driven. After accounting for the effect of greening, we found that scarce winter cumulative precipitation had positive impacts on productivity and respiration, suggesting a possible role of reduced snowpack on the cycling of organic matter. Other variables (i.e., solar irradiance, air temperature, soil moisture, vegetation composition and topography) either supported our expectations or showed no significant effect. Our results contribute to identify the causal relationships between climate and diurnal carbon cycling, improving our understanding of how climate change affects alpine ecosystems in these high-elevation environments.

1 | Introduction

High-mountain areas act as fundamental regulators of the regional climate and the water cycle (Hock et al. 2019). Mountain grassland and shrubland ecosystems store large amounts of organic carbon (i.e., 60.5–82.8 PgC, globally; Ward et al. 2014), representing approximately 3% of the recent carbon stored as living biomass and dead organic matter in the terrestrial biosphere reservoir (Ciais et al. 2014). However, these ecosystems are increasingly threatened by climate changes, with negative

effects on their value as carbon reservoirs. Owing to a set of climate feedback mechanisms (e.g., snow-albedo, cloud or aerosol feedbacks; Pepin et al. 2015), climate changes are amplified in mountains, which display systematic differences in the rates of change in temperature and precipitation with elevation when compared to the surrounding lowlands (Pepin et al. 2022). For this reason, mountain regions have been experiencing particularly harsh changes during the last decades, with decreased snow-cover duration and earlier snowmelt (Niittynen et al. 2020; Rumpf et al. 2022; Marta et al. 2023), accelerated glacier mass loss and retreat (Zemp et al. 2015; Hugonnet et al. 2021; Rounce et al. 2023) and, even if no clear global pattern was identified, changes in summer precipitation gradients (Pepin et al. 2022).

High-elevation grasslands and alpine tundra act as regulators of the hydrological cycle, stabilise slopes, and have a fundamental role in nutrient and carbon cycling (Körner 2004), but climate and environmental changes can deeply influence alpine vegetation and soil microbiota. Rising temperatures, decreased snow-cover and changes in precipitation regimes are favouring upslope migration of some species (e.g., Lenoir et al. 2008), and causing phenological mismatches (e.g., Vitasse et al. 2021) and functional rearrangements (e.g., Bjorkman et al. 2018), thus partially restructuring community composition and possibly altering ecosystem structure and functioning (Descombes et al. 2020). One of the most impressive and widely documented climate-related changes in high-mountain areas is the generalized increase in vegetation cover (i.e., the increase in green vegetated surfaces), a process often referred to as 'greening'. This process was first detected in satellite observations of the Arctic tundra during the late 1990s and thenceforth was identified in high-mountain areas worldwide (Anderson et al. 2020; Choler et al. 2021, 2025; Rumpf et al. 2022). Even if uncertainties exist about the general trend and scale of the process (Myers-Smith et al. 2020), greening is usually thought to be mainly driven by decreased snow-cover duration and increased temperatures (Rumpf et al. 2022). This would favour colonization of previously unvegetated or barely vegetated surfaces, increased plant growth and changes in functional traits, such as leaf area or plant height (Myers-Smith et al. 2020 and reference therein), finally leading to an overall increased productivity.

Vegetation and microbiota participate in the carbon cycle, determining the balance between carbon dioxide uptake due to photosynthesis and carbon release, mainly due to plant respiration and soil microbial activity. Changes in primary productivity have direct impacts on ecosystem functioning, soil temperature conditioning, and nitrogen and carbon cycling (Sistla et al. 2013; Bjorkman et al. 2018; Wang et al. 2023; Maes et al. 2024). These, in turn, have important feedback effects on the regional climate, with alpine ecosystems acting as sinks (or sources) of CO_2, thus mitigating (or not) anthropogenic emissions. The difference between the CO_2 released by microbial decomposition and plant respiration (collectively called ecosystem respiration—ER) and that fixed by plants via photosynthesis (gross primary productivity—GPP) is the net ecosystem exchange (NEE), which measures to what extent an ecosystem functions as a carbon source or sink (Xiao et al. 2008). Still, whether the direction of the feedback effect is negative or positive depends on both the changes in climate and the local adaptations of alpine vegetation (e.g., steppe vs. meadows) (Wang et al. 2023). In energy-limited (moist) ecosystems, for example, increasing temperatures associated with no change in precipitation might promote vegetation growth, increase GPP and thus the amount of carbon stored in soils (soil organic carbon—SOC), while reducing summer soil temperature (and thus potentially ER, as temperature is the primary driver of emissions) via vegetation shading (negative feedback loop, with decreased atmospheric CO_2) (Sistla et al. 2013). The same conditions of warming and precipitation, on the contrary, might reduce vegetation growth in moisture-limited systems (e.g., alpine steppes), making them weaker sinks, or even sources of CO_2 (positive feedback loop) (Wang et al. 2023). Clearly, the same holds also for a single system when a changing climate and seasonal variations involve crossing physiological thresholds, frequently related to plant water balance, that can make the system moisture- or energy-limited (Karnieli et al. 2019; Fu et al. 2022). Whether this involves a temporary or permanent switch of the system toward a carbon source depends on the frequency and intensity of compound drought and aridity events (Zhou et al. 2019).

Changes in vegetation productivity, in turn, add up to climate change in affecting soil microbial dynamics, and therefore emissions (e.g., Ernakovich et al. 2014; Maes et al. 2024). Although microbial changes are much less understood than plant changes, warming is broadly known to enhance microbial activity, but it can also affect the availability and quality of organic matter, vegetation dynamics and biotic interactions (Donhauser and Frey 2018). Reduced snow-cover and early snowmelt can trigger anticipated transition of soil community from winter (fungal-dominated) to summer (bacterial-dominated) communities and a parallel reduction of microbial biomass (Broadbent et al. 2021). In cold soils, fungi are more efficient than bacteria in processing less degradable soil matter, whereas bacteria mostly feed on fresh carbohydrate inputs and root exudates (e.g., Lyu et al. 2024). This, in turn, may change soil carbon stock both directly, owing to differences between bacterial and fungal emissions, and indirectly, because plant growth relies on the availability of labile compounds degraded by bacterial communities (e.g., Bardgett et al. 2005). Therefore, an anticipated shift in microbial communities may disrupt the temporal coupling between plant-microbial resource demand and supply (e.g., Bardgett et al. 2005). Similarly, temporal decoupling can also be triggered by plant community changes that lately cause shifts in soil community, notably when combined with snow-cover reduction (Broadbent et al. 2024), potentially altering the overall carbon balance.

Identifying the biotic and abiotic processes underlying carbon cycling in alpine grasslands is thus important to characterize (and possibly forecast) the effect of climatic stressors in high-elevation ecosystems (Schmeller et al. 2024). Temperature and snow persistence on the ground have been traditionally considered as the major drivers of vegetation dynamics in high-elevation ecosystems (Walker et al. 1994; Körner 2021). The cumulated energy available for plant growth is usually proxied by the sum of daily average air temperatures above 0°C (growing degree days base 0—GDD_0; e.g., Choler et al. 2021), calculated since the snow melt-out date. Here, we aim at understanding to what extent snow and temperature regulate daytime CO_2 exchanges in alpine ecosystems, and to assess the relative

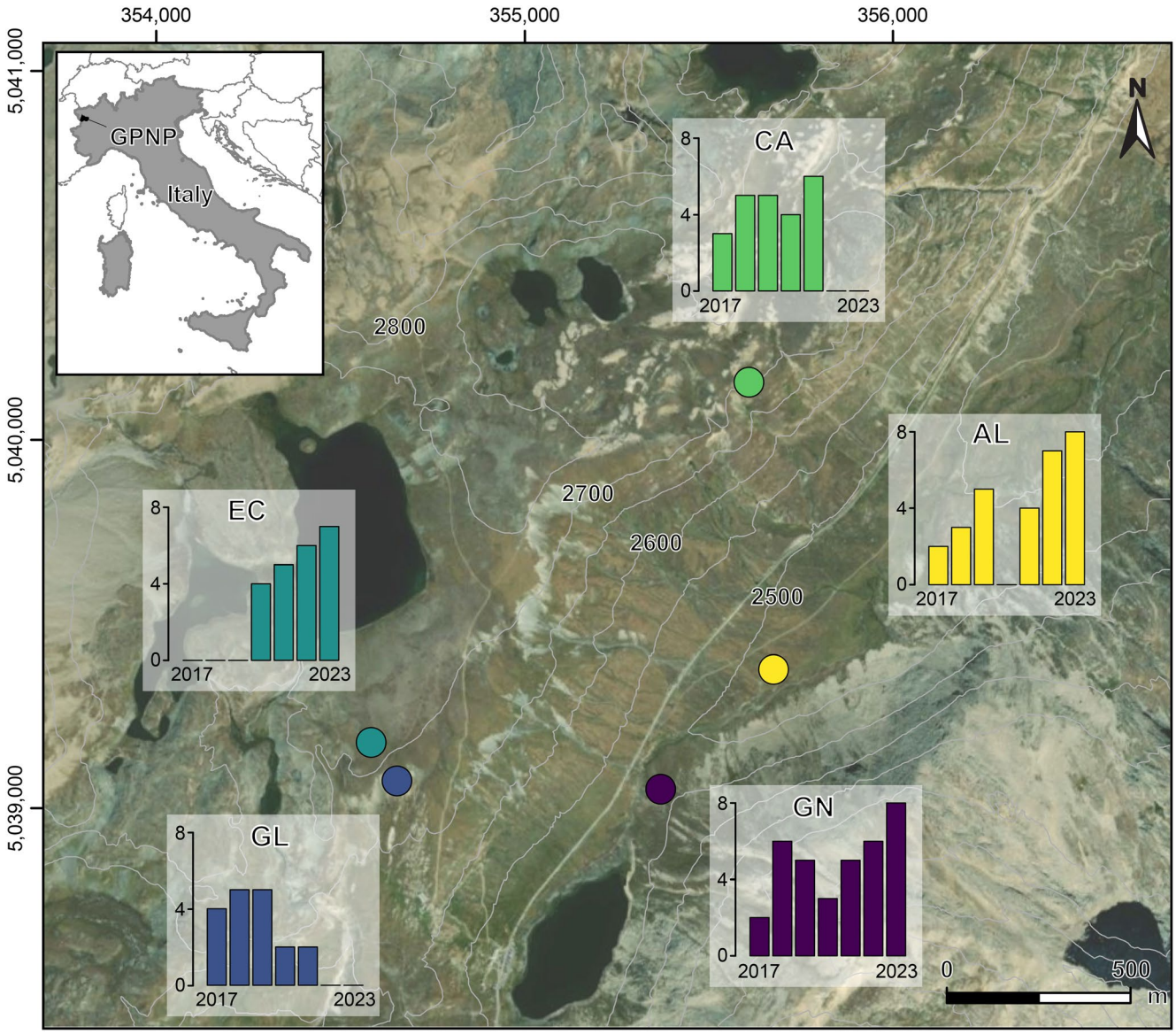

FIGURE 1 | Location map of the five measurement sites (coded as AL, CA, EC, GL and GN) located at the Nivolet Plain in the Gran Paradiso National Park (GPNP, western Italian Alps). For each site, barplots represent the temporal distribution of sampling occasions in the period 2017–2023. Basemap source: Esri, Maxar, Earthstar Geographics and the GIS User Community. Contour lines from the Regional Technical Topographic Map (scale of 1:10,000) available at the Geoportal of the Valle d'Aosta Region (https://geoportale.regione.vda.it/download/ctr/, last access on 17/01/2026). Coordinate reference system: UTM, World Geodetic System 1984, Zone 32 N (EPSG:32632).

importance of energy- and water-related drivers on CO_2 fluxes. To this end, we used a recently published, multi-year dataset with high spatial and temporal resolution (3590 paired NEE and ER diurnal measurements spanning 7 years and five sites; Parisi et al. 2024; Figure 1), and integrated fine-grained environmental information on climate, weather, plant community composition, topography and remotely-sensed vegetation and snow indices with measurements of CO_2 fluxes in high-elevation ecosystems. Specifically, we evaluated the influence of energy- (GDD_0 and air temperature) and water- (soil moisture, winter and summer precipitation) related drivers and their interactions on plant phenology, and assessed to what extent phenology mediates the response of primary productivity and daytime ecosystem respiration, while also accounting for the direct environmental effects on carbon fluxes.

2 | Materials and Methods

2.1 | Fluxes and In Situ Measured Dataset

We used the dataset of CO_2 flux, soil and weather measurements presented in Parisi et al. (2024). Between 2017 and 2023, CO_2 fluxes were measured from five sites located at the Nivolet Plain (Gran Paradiso National Park, Graian Alps, western Italian Alps), spanning between 2549 and 2802 m a.s.l. (Figure 1). The sites, identified by the codes AL, CA, EC, GL, and GN, have different geological and geomorphological characteristics, and were selected to represent the main features observed within the Nivolet Plain (Lenzi et al. 2023 and references therein). AL (2535 m a.s.l.) is located close to the valley floor and is characterized by soils enriched by alluvial and colluvial deposits. GL and

EC (2730 and 2759 m a.s.l., respectively) have soils developed on glacial tills, while CA (2747 m a.s.l.) and GN (2580 m a.s.l.) are characterized by soils developed on carbonatic and metasedimentary parent materials, respectively (Baneschi et al. 2024; Parisi et al. 2024).

A total of 3590 paired NEE and ER measurements were collected, by portable non-steady state (transparent) accumulation chambers equipped with LICOR 850 IRGAs. The transparent chamber allowed to measure NEE, while ER was obtained by shading the chamber with a dark cloth. The GPP was then obtained by subtraction of NEE and ER measurements using the procedures indicated in Baneschi et al. (2023). During each flux measurement, soil and weather sensors recorded continuously soil temperature and moisture as well as air pressure, air temperature, air relative humidity and solar irradiance. Measurements were performed during the snow-free season (i.e., June–October), mainly during the central hours of the day. All sites were investigated for at least 4 years (mean = 5.6, SD = 1.3), with 1 to 8 measurement campaigns per-year carried out in each site (mean = 5.5, SD = 1.7). During each campaign and for each site, ER and NEE were measured in 6–40 individual points (mean = 23.1, SD = 6.4) randomly selected over the site area, for a total sampling time of approx. 2 h per-site. Each measurement point corresponded to a circle with approx. 11 cm radius, while each site covered an area of approx. 16 m radius (mean = 16.4 m, SD = 7.8 m). A complete description of the approaches used to collect field data is reported in Parisi et al. 2024; the full dataset is available at https://zenodo.org/records/10927634 (last accessed on 25/10/2024).

2.2 | Plant Community Composition

Vegetation surveys were conducted in 2019 and 2020, around the seasonal peak of vegetation cover, in order to characterize the overall plant community composition and account for the differing ecological behaviour in terms of carbon fluxes. The percent cover of the main plant species groups, as well as estimates of aerial dry and green biomass, associated with each flux measurement (i.e., within each 11 cm circle), were visually assessed for 173 sampling points randomly selected among those where CO_2 fluxes were measured. The following five plant groups were identified: mosses and lichens (including bare soil), legumes, other forbs, narrow-leaved graminoids (e.g., *Nardus stricta, Festuca* gr. *rubra, Carex curvula*), and medium-leaved graminoids (e.g., *Phleum alpinum, Alopecurus gerardii, Poa alpina*) (Mainetti et al. 2023). Per-site summary information on percent cover for each group is reported in Table S1. To reduce dimensionality and identify the major axes of variation in plant assemblages we performed a discriminant analysis of principal components (DAPC; Jombart et al. 2010), based on percent cover of the various vegetation and biomass classes. Before running the analysis, percent cover data were square-root transformed and scaled to zero mean and unit variance. All the PCA axes were used to run the linear discriminant analysis. The first two DAPC-axes (linear discriminants; LDs) accounted for approx. 91% of the between-group variation, with LD1 representing the most of it (69%; Figure S1). Single plant species groups unevenly contributed to the different axes; LD1 represented a gradient in overall vegetation cover (high percentages of green biomass and legumes vs. bare soil and other forbs). On the other hand, LD2 was mainly driven by the transition from narrow-leaved to medium-leaved graminoids. We thus retained the scores along both LDs as informative proxies of the inter-site differences in plant community (com_1 and com_2).

2.3 | Remotely-Sensed Factors: Snow, Climate, Topography and Vegetation Indices

Snow cover is one of the main determinants of vegetation dynamics in high-elevation ecosystems (Niittynen et al. 2020). To identify the occurrence of snow on the ground, and consequently the days of snowmelt and snowfall, regulating the length of the growing season for plants, we used the NDSI-derived, coarse-grained MODIS Terra 500 m daily fractional snow cover (Hall et al. 2016; available at https://developers.google.com/earth-engine/datasets/catalog/MODIS_006_MOD10A1). This product is already masked for clouds, ocean and night; liquid water (i.e., lakes) was not an issue in our case, as the cells considered had limited (≈1.1%) or no intersection with water bodies. Following Niittynen and Luoto (2018), we (i) identified the satellite pixels including each individual measurement; (ii) converted fractional snow cover to occurrence using the threshold of 40% (i.e., snow was assumed to be present when the fractional snow cover was at least 40%; Macander et al. 2015); (iii) fitted a binomial generalized linear model (GLM) within each pixel (time-series of observed presence-absence of snow on the ground) to map the probability of snow occurrence through time, and (iv) identified the day when this probability was closer to 0.5 as the day of snowmelt (or snowfall). The fitting was iterated over each year and for two timeframes (snowfall: 1st October of the previous year to 31st March, and snowmelt: 1st April to 30th September). This allowed us to calculate for each cell and year several metrics: the days of snowfall for the previous year, snowmelt and snowfall, and the length of the 'summer' (snow-free) and 'winter' (snow-covered) seasons.

To account for the effects of climate on vegetation dynamics, we built on daily temperature and precipitation recordings from the close Lago Serrù weather station (2275 m a.s.l.; average distance from sampling points = 3788 m; SD = 449 m; data available upon request from Iren S.p.A.). Based on yearly information on snowmelt dates, we calculated the cumulated energy available for plant growth as the sum of daily average air temperature above 0°C (growing degree days base 0—GDD_0; Choler et al. 2021) between the snowmelt and each sampling date. Specifically, GDD_0 was calculated for each point based on the sum of the daily average temperatures since snowmelt, after excluding all the daily averages with minimum temperature lower than the base temperature (i.e., 0). 'Summer' precipitation ($meanP_s$) was calculated as the average daily amount of liquid precipitation received since snowmelt, until the sampling date, whereas 'winter' precipitation ($cumP_w$) was simply the sum of solid precipitation fallen between the snowfall date of the previous year and the snowmelt. Before calculating GDD_0, the temperatures recorded at the Lago Serrù station were adjusted by applying the standard average temperature lapse rate of −0.0065°C/m (Barry 2008) to account for the altitude-dependent decrease of temperature between the weather station and the sampling sites. Conversely,

precipitation was assumed not to differ (in terms of total volume, not state—i.e., liquid or solid) between the weather station and the sampling sites. That is, all sites were assumed to receive the same amount of precipitation, and estimates of winter and summer amounts differed only owing to sampling dates and start of the growing season (i.e., snowmelt date). Small differences might occur between sites due to the complex topography of the area and the differences in elevation (maximum elevation gap 253 m). To obtain proxy measures of water accumulation/discharge dynamics and snow accumulation/removal by wind due to differences in topographic setting, we used a multiscale topographic position index (*mTPI*; Theobald et al. 2015) derived from the TINITALY v1.1 digital elevation model (DEM, 10 m resolution; Tarquini et al. 2007; Tarquini et al. 2023). For each cell, we iteratively calculated its position relative to the surrounding cells in a circular area with fixed radius, based on four distance classes (radius of 10, 40, 400 and 1000 m); the index was finally obtained as the average of the results for the four distance classes. This approach allowed integrating the effect of topography with changing spatial scale, thus discriminating between, for example, sampling points located in small depressions but close to mountaintops, and sites close to the valley floor. In general, the resulting *mTPI* showed a high correlation with DEM (Pearson's $r = 0.61$; $r = 0.97$ when considering only the sampling points).

Several vegetation indices (*VIs*) were calculated to account for differences in vegetation cover between sites and vegetation phenology between years, based on the Sentinel-2 Multispectral product (available at https://developers.google.com/earth-engine/datasets/catalog/COPERNICUS_S2_SR_HARMONIZED) at 10 or 20 m resolution, depending on the band used. The selected indices focus on slightly different properties of vegetation and refer to different aspects of vegetation productivity (Zeng et al. 2022). Specifically, the normalized difference vegetation index (Tucker 1979):

$$NDVI = (NIR - RED) / (NIR + RED)$$

and the near-infrared reflectance of vegetation (Badgley et al. 2017):

$$NIRv = ((NIR - RED)/(NIR + RED)) \times NIR$$

mainly focus on vegetation structure, whereas the red-edge chlorophyll index (Gitelson et al. 2003):

$$CIred - edge = (NIR / red - edge) - 1$$

provides information on the chlorophyll content and mainly focuses on plant physiology and biochemical properties (Zeng et al. 2022).

To account for the effect of cloudiness on vegetation indices, for each individual sampling point we estimated the proportion of terrain classified as 'vegetated' or 'bare soil' by the Sentinel-2 scene classification map (SCL classes 4 and 5, respectively) within a radius of 50 m, for all the images available in the 15 days before and after the sampling date. We finally selected (if any) the temporally closest image with a proportion of cloud-free terrain higher than 0.95. All the spatial analyses were run in R using the *raster* package (Hijmans 2022); remotely-sensed data were retrieved using Google Earth Engine and the *rgee* package (Aybar et al. 2020).

2.4 | Statistical Analyses

Given the fine-grained intrinsic variability of individual measurements of CO_2 fluxes and some of the environmental variables, we followed Magnani et al. (2020) and averaged all individual measurements in each site from the same sampling occasion (site × date; 150 sampling occasions). Before averaging, all measurements with a proportion of cloud-free terrain < 0.95 were excluded, and average values were calculated only for sampling occasions with ≥ 15 individual measurements. Independent variables were chosen to represent causal relationships between CO_2 fluxes (both ER and GPP) and the environment, trying to fully account for the spatial, temporal and spatio-temporal sources of variation. Community composition (com_1 and com_2) and *mTPI* were thought to mainly account for inter-site differences, and to have no variability along the season and across years. Similarly, cumulative winter precipitation ($cumP_w$) accounts for inter-site differences, was thought to change across years, but not along the season. Cumulated heat (GDD_0), average summer precipitation ($meanP_s$) and vegetation indices should account for inter-site and date differences (i.e., change along the season, among sites and across years), but have a limited variability related to single measurements. Finally, air temperature (*airT*), solar irradiance (*swrad*) and soil moisture (*soilVWC*) were thought to represent the fine-scale, instantaneous variability, intrinsically related to individual measurement points (i.e., they vary even within single sampling occasions). Air relative humidity and air pressure were excluded from the set of predictors as they were previously found to either barely influence fluxes or reflect elevational gradients (Magnani et al. 2020; Lenzi et al. 2023), while soil temperature was not included in the model due to a high proportion of missing values; however, given its strong correlation with air temperature, we retained *airT*, benefiting from its more complete data coverage.

We used piecewise structural equation models (pSEMs; Lefcheck 2016) to evaluate the direct and indirect effects of environmental variability on the measured CO_2 fluxes. By convention, ER has positive values, and GPP ($GPP = NEE - ER$) is negative, possibly leading to counterintuitive relationships; therefore, we used its absolute value (|GPP|) in all the analyses. SEMs require the definition of an a priori model, describing the shape and direction of potential relationships between variables. We hypothesized the same conceptual structure to hold for both ER and |GPP|, with the only difference that respiration depended positively and linearly on air temperature, and productivity on solar irradiance. We expect increasing values of the vegetation index and a larger water supply (in terms of soil moisture, winter and summer precipitations) to enhance both productivity and, by promoting at least the autotrophic component of ER, ecosystem respiration. We also expect higher proportions of both vegetation cover (com_1) and medium-leaved graminoids (com_2) to possibly reflect a gradient in biomass and soil nutrients (Jiang et al. 2017; Mainetti et al. 2023—i.e., healthier and more

productive vegetation corresponding to higher values of com_1 and com_2), and hence positively influence |GPP| and the autotrophic component of ER. Finally, a non-linear (Beta) relationship between CO_2 fluxes and cumulated heat (βGDD_0) was included to account for the expected effect of cumulated heat in regulating both plant growth and senescence, and overall vegetation activity along the snow-free season in high-elevation areas (Möhl et al. 2022; Choler et al. 2025). Specifically, the Beta relationship allows estimating two separate shape parameters, here representing the growth and senescence phases, so accounting for the different rates of vegetation change during the first and last parts of the season. In turn, instantaneous air temperature (*airT*) was expected to be linearly and positively dependent on solar irradiance, on GDD_0 (reflecting temperature changes along the season), and negatively on *mTPI*, reflecting the decrease of temperature with elevation. Instantaneous soil volumetric water content (*soilVWC*) was expected to be negatively dependent on *airT* and GDD_0, while positively on the amount of winter and summer precipitations. For both water-related variables (i.e., $meanP_s$ and $cumP_w$), an interaction with *mTPI* was included to represent the differential effect of microtopography on water accumulation and discharge dynamics. Finally, vegetation indices were expected to be positively dependent on community composition and seasonal water supply ($meanP_s$ and $cumP_w$). Also in this case, the effect of cumulated heat was expected to be non-linear (βGDD_0). Two-terms interactions between βGDD_0 and community composition, winter cumulative ($cumP_w$) and summer ($meanP_s$) precipitation were included to represent the differential effects that heat exerts with varying levels of vegetation cover or water supply. A detailed list of all variables used, along with their origin and the spatial and temporal scales at which they are supposed to influence the processes, can be found in Table S2.

To identify the shape parameters of the Beta distribution for each vegetation index, we fitted preliminary non-linear mixed-effect models using the *nlme* R package (Pinheiro and Bates 2000). The general model took the form:

$$VI = b_0 \frac{\Gamma(\alpha+\beta)}{\Gamma(\alpha)\Gamma(\beta)} GDD_0^{\alpha-1}\left(1-GDD_0\right)^{\beta-1}$$

where *VI* is the vegetation index (summarizing vegetation activity along the snow-free season), and site identity acted as random effect on the scaling term (b_0) of the Beta function. This formulation allowed us to account for inter-site differences in environmental variables other than GDD_0 possibly influencing *VIs*, without explicitly modelling them at this step. Finally, the estimated shape parameters (i.e., α and β) were used to transform GDD_0, so to allow fitting a non-linear term within the linear framework available in pSEM. The parameter estimation was repeated for each vegetation index, and GDD_0 was Beta-transformed accordingly; this led to three equivalent SEMs, only differing for the vegetation index integrated in the sub-models and the corresponding βGDD_0.

Before running SEMs, all variables were scaled to zero mean and unit variance, and collinearity was evaluated within each single sub-model using simple linear models and standard or generalized (in case of interactions) variance inflation factors (*car* package; Fox and Weisberg 2019). All VIFs (i.e., VIF or $(GVIF^{1/(2\times df)})^2$) were low ($VIF_{max} = 3.21$), indicating that multicollinearity did not pose major issues (i.e., regression coefficients were reliably estimated and identified effects were stable in terms of direction and magnitude). Residuals from each sub-model fairly approximated normal distributions (Shapiro–Wilk test; $W_{min} = 0.94$). Fisher's C statistic was used to test the goodness-of-fit of piecewise SEMs. Full model specification, including all covariations, is reported in Text S1. Additionally, to evaluate the combined contribution of individual predictors to both additive and interactive terms within each sub-model of each SEM, we implemented a randomization test following Thuiller et al. (2009). Pearson's correlation coefficient (r) was used to compare the predictions obtained using original and randomized variables; for each permutation, variable importance was finally expressed as $1 - r$. Predictions were generated using coefficients estimated by SEMs for each sub-model separately. To assess possible overfitting issues, the final model was rerun by using the complete dataset (i.e., single point measurements) and coefficients obtained from this analysis were compared. To account for non-independence of single observations, we used linear mixed effect models with a nested random intercept structure (i.e., intercept varying among sites, among years within each site and among sampling occasions within each site and year). To reduce heteroskedasticity in the residuals from each sub-model, an exponential variance function structure was implemented using the *nlme* R package (Pinheiro and Bates 2000). All the analyses were run using R version 4.4.2.

3 | Results

After removing records with missing information (e.g., unreliable *VIs* due to cloudy scene) and sampling occasions with <15 records, a total of 2917 individual measurements of CO_2 fluxes were retained, resulting in 127 sampling occasions over 7 years (per-site mean = 25.4, SD = 6.66; per-year mean = 18.14, SD = 4.49). For each sampling occasion, the number of individual measurements ranged between 15 and 40 measurements (per-sampling occasion mean = 22.97; SD = 5.97).

Yearly × site-averaged values of the recorded fluxes ranged within [−13.21, −5.00] μmol $m^{-2}s^{-1}$ for GPP and [2.68, 7.79] μmol $m^{-2}s^{-1}$ for ER, in line with previous observations from the same sites (Magnani et al. 2020; Lenzi et al. 2023; Vivaldo et al. 2023).

The date of snowmelt ranged widely during the timeframe of interest (Figure S2a; DOY = [130,180], mean = 162, SD = 13), with 2022 characterized by an exceptionally early (approx. half May) melting over the whole study area. It is worth noting here that the different sites all belonged to different MODIS cells, but the quite coarse spatial scale of this product might obscure local (i.e., within-cell) variations in the timing of snowmelt, mainly due to differences in snow accumulation by wind, aspect and ruggedness (Erickson et al. 2005). When expressed relative to the snowmelt date, CO_2 fluxes and vegetation indices (Figure S2b–f, respectively) showed clear temporal patterns, mainly corresponding to the seasonal development, maturity and senescence of vegetation. A clear seasonal pattern is also evident for soil moisture (Figure S2g), with initially high values due to snowmelt, a decline in the

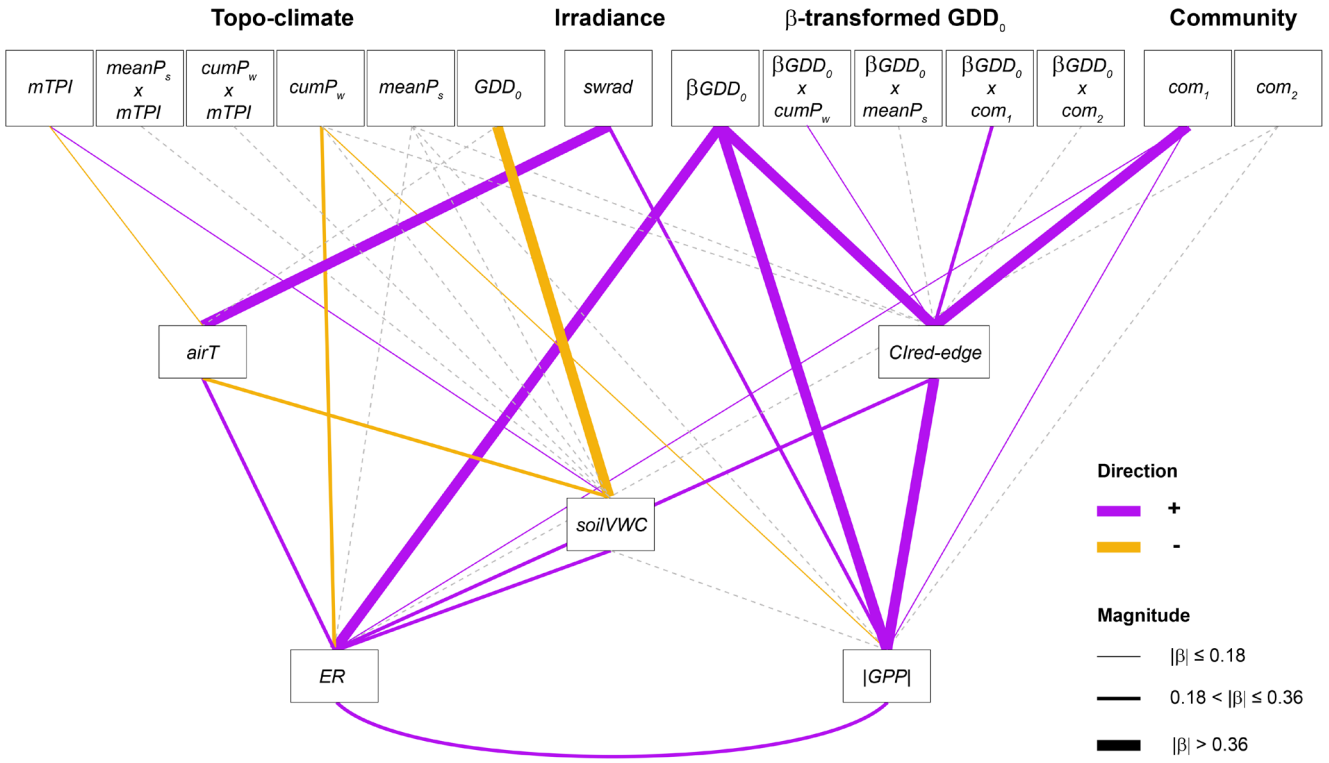

FIGURE 2 | Direct and indirect effects of climate, topography and community composition on vegetation indices, soil moisture, air temperature and CO_2 fluxes. The model reported here is based on the *CIred-edge* vegetation index; coefficients for models integrating *NDVI* or *NIRv* are reported in Table S3. Apart from the covariation between ER and |GPP|, all relationships must be interpreted as directional (top to bottom, with exogenous variables on the first row of the diagram). Line width indicates the absolute magnitude of standardized coefficients ($0 \leq$ thin ≤ 0.18, $0.18 <$ medium ≤ 0.36, $0.36 <$ tick ≤ 0.74), while colours represent the direction of the relationship. Dashed grey lines mark non-significant relationships. βGDD_0, Beta-transformed GDD_0; *airT*, air temperature; *CIred-edge*, remotely-sensed red-edge chlorophyll index; com_1, vegetation cover; com_2, proportion of medium-leaved graminoids; $cumP_w$, cumulative winter precipitation; *ER*, ecosystem respiration; GDD_0, growing degree days base 0; *GPP*, gross primary productivity; $meanP_s$, average summer precipitation; *mTPI*, multiscale topographic position index; *soilVWC*, soil moisture; *swrad*, solar irradiance. *x* marks interactions between variables (products).

dryer months and a second increase toward the end of the summer season. Air temperature (Figure S2h) showed no clear pattern, but a slightly increasing spread as the summer progressed.

The conceptual models developed to identify the direct and indirect effects of environmental drivers on vegetation indices, soil moisture, air temperature and CO_2 fluxes were well supported by the data ($12.40 \leq$ Fisher's $C \leq 15.38$, with $0.12 \leq p$ value ≤ 0.26; Figure 2 and Table S3). Sub-models for fluxes and vegetation development showed satisfactory performances, with R^2 for vegetation indices ranging within [0.68, 0.80], for |GPP| within [0.74, 0.81] and for ER within [0.50, 0.58], while models for soil moisture and air temperature showed poorer fits (0.33 and 0.16, respectively). Air temperature (*airT*) showed a positive and strong relationship with incoming solar irradiance (*swrad*), and a negative relationship with topography (*mTPI*), with no significant effect of cumulated heat (GDD_0) (Figure S3). Increasing GDD_0 and *airT* were found to decrease soil moisture (*soilVWC*), while increasing *mTPI* had a positive effect; no significant effect was found for both winter and summer precipitation ($cumP_w$ and $meanP_s$, respectively), and the interactions between *mTPI* and precipitation (Figure S4). Vegetation indices showed an overall consistent pattern among SEMs, with strong and positive effects of βGDD_0, vegetation cover (com_1) and their interaction, indicating that increasing percent cover boosts the relationship between *VIs* and βGDD_0. Similarly, all *VIs* returned a significant effect of the interaction between $cumP_w$ and βGDD_0, reflecting a more pronounced seasonality when winter precipitation was heavier. No statistically significant effects of either $meanP_s$ or com_2, or their interaction with βGDD_0 were detected (Table S3 and Figure S5).

Even though the same conceptual sub-model was used for ER and |GPP|, differences were found in the drivers of CO_2 fluxes (Figures S6 and S7). Vegetation indices (*CIred-edge, NDVI*, or *NIRv*) were always identified as major drivers for |GPP| but had minimal or no influence on ER. Similarly, the positive effect of soil moisture was found for ER only. We found $cumP_w$ to be negatively related to both ER and |GPP| (Table S3), while the increase in vegetation cover (increasing com_1) had positive effects on both fluxes. Increasing *airT* and *swrad* increased ER and |GPP|, respectively. Finally, the effect of βGDD_0 was always significant and positive for both |GPP| and ER, while both com_2 and $meanP_s$ had no significant effect on fluxes.

Covariation between pairs of exogenous variables (i.e., correlation) was significant and moderate to high ($0.35 \leq |$ Pearson's $r| \leq 0.75$), both for Cov(GDD_0 and βGDD_0) and for site-levels

attributes (com_1, com_2 and *mTPI*). Significant covariations between exogenous and endogenous variables (i.e., residual correlations) mainly identify relationships not included in the models to avoid collinearity issues (e.g., Cov(*ER*, *swrad*)), or relationships due to underlying processes influencing two variables, but with no causality (e.g., both *VIs* and *swrad* change along the season following a hump-shaped trend). Finally, the residual correlation between the endogenous ER and |GPP| was positive and significant ($0.36 \leq$ Pearson's $r \leq 0.50$). Estimated regression coefficients and covariations for models integrating different vegetation indices are reported in Table S3. The comparison of SEM coefficients estimated when integrating indices alternative to the *CIred-edge* (i.e., *NDVI* and *NIRv*) is reported in Figure S8. Looking at the contribution of single predictors to sub-models (i.e., direct effects only; Figure S9), we found βGDD_0 (in interaction with com_1) to explain the most part of variation in vegetation indices (Figure S9g–i), and importantly contributing to the model on CO_2 fluxes (|*GPP*| and *ER*; Figure S9a–f). Vegetation indices (*VIs*) and *swrad* largely contributed to sub-models on |*GPP*| (Figure S9a–c), while the effect of *VIs* was reduced in the sub-models for ER (Figure S9d–f), where *soilVWC* and βGDD_0 played a major role. Finally, GDD_0 and *swrad* resulted to be the main drivers for soil moisture (*soilVWC*; Figure S9j) and *airT* (Figure S9k), respectively. The model based on single point measurements returned largely comparable results, in term of regression coefficients (Figure S10), but generally lower performances in terms of marginal R^2 ($0.03 \leq R^2_m \leq 0.78$).

4 | Discussion

Vegetation dynamics in high-elevation ecosystems are mainly regulated by temperature and snow persistence on the ground (Walker et al. 1994; Körner 2021). Our results show how these factors also play a major role in controlling daytime CO_2 fluxes; water-related drivers, on the contrary, returned weaker signals, indicating primarily an energy limitation in our study system. Cumulated heat since snowmelt, in fact, emerged as the main climatic regulator of the amount of carbon stored in plants and soils or released into the atmosphere as carbon dioxide during the day (i.e., the diurnal net ecosystem exchange). In case nighttime ER would be analogously influenced by GDD_0, this would heavily condition the efficiency of the system in acting as carbon sink and mitigate anthropogenic CO_2 emissions.

4.1 | Cumulated Heat, Phenological Development and CO_2 Fluxes

Our results highlight that cumulated heat since snowmelt (GDD_0) represents one of the most important predictors also for ER and GPP. In fact, Beta-transformed GDD_0 overtakes the effect of the most used predictors of ER and GPP, namely temperature and solar irradiance, respectively. The effect of βGDD_0 on the fluxes was both direct and mediated by vegetation indices (Figure 2; Figure S9a–i, respectively). After accounting for seasonal and inter-annual fluctuations of vegetation phenology and cover using remotely-sensed vegetation indices, we found cumulated heat still influencing diurnal CO_2 fluxes (Figures S6c and S7d). This suggests that GDD_0 summarizes a variety of different environmental and physiological effects and can be considered, at least for these high-altitude ecosystems, as the main proxy of the set of control variables.

The effect of vegetation indices was particularly strong for gross primary productivity (Figure S9a–c), with its influence on GPP being as important as βGDD_0. In contrast, for ER, vegetation indices are far less important than βGDD_0. It is well known that vegetation indices exhibit non-linear responses to aboveground biomass or plant cover when dense, stratified canopies occur (i.e., *VIs* suffer from signal saturation—Myneni and Williams 1994). We may thus interpret the support of the partial mediation model for primary productivity ($\beta GDD_0 \rightarrow VIs \rightarrow |GPP|$ and $\beta GDD_0 \rightarrow |GPP|$) as the effect of GDD_0 on the different axes of plant growth (i.e., the planar and vertical ones, in agreement with Happonen et al. 2022), indirectly accounting for the total aboveground biomass. As a simplification, we can assume that vegetation begins to grow just after snowmelt, with local increase in greening (detected by vegetation indices). At the same time, vegetation height starts to increase, continuing until plant maturity (which often occurs long after total coverage is reached), leading to complex and stratified canopies that saturate the spectral signal. Beyond GDD_0, the other factor that mostly influence vegetation indices is com_1, representing the proportion of green biomass and legumes within the flux measurement area. Notice that this predictor has an indirect (mediated by *VIs*) effect on both fluxes, as well as a weak direct effect. Local differences in community composition, abundance and plant functional traits (mainly plant height, aboveground biomass, leaf area index and leaf orientation; Sellers 1985; Myneni and Williams 1994; Huete et al. 2002) condition and shape the observed relationships, with sparsely vegetated areas or areas with dwarf vegetation that are less prone to signal saturation (Choler et al. 2021). The positive direct effect that a high proportion of legumes and green biomass (i.e., high values of com_1; Table S3) has on the fluxes may thus reflect more structured canopies, accounting for the portion of variance left unexplained by the partial mediation model. In other words, local assemblages differ by total cover, influencing their spectral response, but also by biomass and canopy structure, influencing their productivity and autotrophic respiration at equal spectral response.

4.2 | Water Dynamics

The predictors with a relatively lower importance (standardized coefficients between 0.18 and 0.36) were mostly linked to meteoclimatic variability; still temperature, winter precipitation and soil moisture, and solar irradiance played important roles for ER and GPP, respectively. We found no significant effect of the cumulated heat since snowmelt (GDD_0) on the instantaneously measured air temperature. Instead, this latter is strongly dependent on the instantaneously measured solar irradiance, possibly reflecting a dependence of air temperature more on the conditions during the measurement (mainly hour of the day and cloud cover) than on the seasonal trend of temperature. In turn, air temperature and, to a larger extent, cumulated heat influenced soil moisture, likely capturing the dynamics of seasonal and daily-to-hourly changes of evapo(transpi)ration-driving factors, respectively. Finally, winter precipitations negatively influenced both ER and GPP, with a stronger effect for ER. While the effect

of temperature and solar irradiance on ER and GPP is well established, our results reveal a more complex picture of water dynamics, warranting additional consideration.

Winter and summer precipitation amounts have multiple effects on carbon cycling in alpine ecosystems: they directly and indirectly affect both gross primary productivity and ecosystem respiration by conditioning vegetation growth (e.g., Choler et al. 2025), phenology (e.g., Möhl et al. 2022), community composition (e.g., Liu et al. 2018), biomass production (e.g., Bai et al. 2004) and nutrient cycling (e.g., Chen et al. 2022). Our precipitation proxies, based on timeseries from a single weather station, might fail to fully account for the small-scale dynamics of precipitation (e.g., snow accumulation by wind) and this, in turn, might partly explain the contrasting signals about the effects of water availability on this alpine grassland. We found no statistically significant effect of average summer precipitation, considering both soil moisture and vegetation phenology and productivity (Figure 2; Table S3). However, we detected a tendency to increasing soil moisture with increasing summer precipitation for sites with low *mTPI* (i.e., close to valley floor—Figure S4a), supporting the idea of short-term accumulation/discharge dynamics due to topographic setting. Soil moisture, in turn, proved to be one of the stronger drivers of ecosystem respiration (Figure S7c; Figure S9d–f), but had no effect on productivity (Figure 2; Table S3). When looking at the effect of winter precipitation, we found no effect on soil moisture, possibly reflecting the absence of long-term accumulation of water from snow melting, but we detected negative direct effects on CO_2 fluxes (Figure 2; Table S3). We might hypothesize that the latter effect is plausibly due to increased nutrient mobilization due to reduced snow cover, rather than to a decreased water supply at the beginning of the season. Indeed, a poorly developed (< 30 to 40 cm in depth) snow cover reduces the insulating effect of snow on soil, and results in the increase of freeze/thaw cycles (Edwards et al. 2007). Owing to the adaptations of local microbial communities to the harsh alpine conditions, it is highly improbable that freezing episodes directly influence the microbial community, inactivating most of the microbial biomass and reducing respiration in the subsequent growing season. On the contrary, these events might significantly increase physical litter and soil disruption, leading to an increased nutrient mobilization (Freppaz et al. 2007). This, in turn, may result in an increased nutrient availability for plants and microbial communities during the subsequent growing season (Viglietti et al. 2014), and hence possibly lead to increased plant productivity and ecosystem respiration. When analysing the effect of summer precipitation on vegetation indices and CO_2 fluxes, we have to consider the composition of local communities. Depending on the life form, Winkler et al. (2016) found contrasting responses to soil moisture. Increasing water availability decreased the aboveground primary productivity of forbs and succulents, but increased that of graminoids and cushion plants, possibly depending on the species adaptation and the local microclimate. Xu and Zhou (2011) however, found non-linear, hump-shaped responses of biomass production and CO_2 assimilation rate to increasing precipitation in two graminoid species, possibly related to both water stress and excessive water loads. In our study system, we found percentages of dicotyledons at the peak cover substantially balancing those of graminoids (within-site mean: 35% to 55% vs. 36% to 45%; SD: 18% to 27% vs. 17% to 24%, respectively), making difficult to disentangle differential contributions to fluxes under different moisture regimes.

4.3 | Autotrophic and Heterotrophic Contributions to ER

Owing to their physiological links (Waring et al. 1998; Janssens et al. 2001; Kuzyakov and Gavrichkova 2010; Jian et al. 2022), gross primary productivity and ecosystem respiration showed a high correlation (Pearson's $r = 0.75$; residual correlation: $0.36 \leq$ Pearson's $r \leq 0.50$). On the other hand, several conspicuous differences emerged, in terms of both model goodness-of-fit ($|GPP|$: $0.74 \leq R^2 \leq 0.81$ vs. ER: $0.50 \leq R^2 \leq 0.58$) and differential variable contribution to models (Figures S6, S7 and S9a–f). In particular, the partial mediation model of *VIs* is weaker for ecosystem respiration compared to productivity ($\beta GDD_0 \rightarrow VIs \rightarrow$ CO_2 flux—total effects, interactions excluded: $0.25 \leq |GPP| \leq 0.32$ vs. $0.02 \leq ER \leq 0.17$; Table S3), indicating that diurnal respiration is mainly driven by variables other than plant phenological status (i.e., cumulated heat, air temperature and soil moisture). The surprising lack of a significant effect of instantaneously-measured soil moisture on $|GPP|$ can be due to complex cross-correlations: *soilVWC* depends on GDD_0, and this in turn covariates with βGDD_0 (Pearson's $r = -0.75$; Table S3). βGDD_0, on the other hand, influences both *VIs* and CO_2 fluxes, with a stronger effect for $|GPP|$, thus possibly obscuring the direct effect of *soilVWC* on primary productivity. As ecosystem respiration accounts for both autotrophic and heterotrophic emissions, disentangling their relative contribution and measuring the differential effects that environmental changes might have on each component is complex (Bond-Lamberty et al. 2004). A tight, positive relationship between autotrophic respiration and primary productivity is expected (Janssens et al. 2001; Hicks Pries et al. 2015). Still, increased productivity also involves an increasing biomass, and hence more organic carbon could be sent to soil in form of, for example, dead roots or litter; in turn, this might promote heterotrophic respiration (Giardina et al. 2014; Maes et al. 2024). Whether this involves a balanced contribution to total ecosystem respiration or not, depends on the existence and strength of a temporal disconnection between SOC formation and microbial carbon consumption. Several studies reported heterotrophic respiration lagging behind primary productivity, and mainly depending on the carbon that was fixed one to several years before (Bond-Lamberty et al. 2012; Berryman et al. 2018). Consequently, the weaker signal from vegetation indices in the path to ecosystem respiration might indicate a weaker contribution of contemporary plant productivity to CO_2 efflux, and supports the view that respiration is mainly microbial-driven and temperature-related in this grassland ecosystem.

4.4 | CO_2 Fluxes Under a Changing Climate

The impact of climate change on carbon fluxes in high-elevation ecosystems largely depends on the local climate and the adaptation of the plant and microbial communities (Wang et al. 2023; Maes et al. 2024). However, the response of plant growth and productivity to increasing temperature and precipitation may reach an asymptote (i.e., might stabilize at a certain level) if the plant phenology is primarily determined by genetic factors.

Although earlier snowmelt can extend the potential growing season in alpine environments, plant adaptations to short snow-free periods can instead limit the effective duration of phenological activity. As shown by Möhl et al. (2022), an earlier snowmelt tends to trigger an earlier onset of both growth and senescence, without necessarily increasing root development—at least for the dominant components of alpine vegetation. This trend appears to hold also at larger spatial scales and across different ecosystems (Meng et al. 2024). Whether this will involve, on the short term, a community restructuring will depend on the ability of the species to delay senescence (i.e., elongate their growing season) and both outcompete the others and colonize unoccupied sites (Windmaißer and Reisch 2013). Wang et al. (2023) found that, at least for the Tibetan Plateau, the net carbon uptake increased mainly owing to increased precipitation in water-limited systems (alpine steppes). On the opposite, higher temperatures increased the carbon sink role only for alpine grasslands receiving adequate precipitation during the growing season. Our results on the effects of temperature and precipitation suggest that we are dealing with a temperature/energy- rather than a water-limited system, at least when looking at vegetation phenology and productivity. Unless drastic reductions in the current precipitation volume or changes in precipitation seasonality occurring in conjunction with no restructuring of the local plant communities, our results suggest an increased gross primary productivity and diurnal ecosystem respiration with a warming climate, possibly leading to a more favourable net balance for these alpine grasslands.

Author Contributions

S.M., M.M. and A.P. conceived and designed the study; M.M., G.V., A.M., I.B., A.B., M.S.G., S.R.E., M.L., B.R. and A.P. collected and validated field data; S.M. wrote the codes, conducted the statistical analyses, and produced the illustrations with inputs from M.M., G.V., S.G., S.R.E., M.L. and A.P.; S.M., M.M. and A.P. led the writing with contributions from all the authors.

Acknowledgements

The authors acknowledge Bruno Bassano, Ramona Viterbi and all the staff of GPNP for help and support during the field activities. Francesca Avogadro di Valdengo, Maria Virginia Boiani, Maurizio Catania, Sara Lenzi, Pietro Mosca and Angelica Parisi contributed to data collection and curation. S.M., A.B., S.G., B.R. and A.P. acknowledge the support of the Italian Integrated Environmental Research Infrastructures System (ITINERIS), funded by the European Union in the framework of the NextGenerationEU PNRR Mission 4 'Education and Research'—Component 2: 'From research to business'—Investment 3.1: 'Fund for the realization of an integrated system of research and innovation infrastructures'—Project code IR0000032—CUP B53C22002150006. M.M., I.B., G.V. and A.P. acknowledge the support of the National Biodiversity Future Center (NBFC), funded by the European Union in the framework of the NextGenerationEU PNRR Mission 4 'Education and Research'—Component 2: 'From research to business'—Investment 1.4: 'Strengthening research structures and creating "National R&D champions" on certain Key Enabling Technologies'—Project code CN00000033—CUP B83C22002930006. Open access publishing facilitated by Consiglio Nazionale delle Ricerche, as part of the Wiley - CRUI-CARE agreement.

Funding

This work was supported by the European Union (IR0000032 and CN00000033).

Conflicts of Interest

The authors declare no conflicts of interest.

Data Availability Statement

The data that support the findings of this study are openly available in figshare at https://figshare.com, reference number 10.6084/m9.figshare.28945982.

References

Anderson, K., D. Fawcett, A. Cugulliere, et al. 2020. "Vegetation Expansion in the Subnival Hindu Kush Himalaya." *Global Change Biology* 26, no. 3: 1608–1625.

Aybar, C., Q. Wu, L. Bautista, R. Yali, and A. Barja. 2020. "Rgee: An R Package for Interacting With Google Earth Engine." *Journal of Open Source Software* 5: 2272.

Badgley, G., C. B. Field, and J. A. Berry. 2017. "Canopy Near-Infrared Reflectance and Terrestrial Photosynthesis." *Science Advances* 3, no. 3: e1602244.

Bai, Y., X. Han, J. Wu, Z. Chen, and L. Li. 2004. "Ecosystem Stability and Compensatory Effects in the Inner Mongolia Grassland." *Nature* 431, no. 7005: 181–184.

Baneschi, I., M. Giamberini, M. Magnani, et al. 2024. "Alpine Critical Zone Observations at the Gran Paradiso National Park, Italy." In *Critical Zone and Ecosystem Dynamics*. Springer Nature.

Baneschi, I., B. Raco, M. Magnani, et al. 2023. "Non-Steady-State Closed Dynamic Chamber to Measure Soil CO_2 Respiration: A Protocol to Reduce Uncertainty." *Frontiers in Environmental Science* 10: 1048948.

Bardgett, R. D., W. D. Bowman, R. Kaufmann, and S. K. Schmidt. 2005. "A Temporal Approach to Linking Aboveground and Belowground Ecology." *Trends in Ecology & Evolution* 20, no. 11: 634–641.

Barry, R. G. 2008. *Mountain Weather and Climate*. Cambridge University Press.

Berryman, E. M., M. K. Vanderhoof, J. B. Bradford, et al. 2018. "Estimating Soil Respiration in a Subalpine Landscape Using Point, Terrain, Climate, and Greenness Data." *Journal of Geophysical Research: Biogeosciences* 123, no. 10: 3231–3249.

Bjorkman, A. D., I. H. Myers-Smith, S. C. Elmendorf, et al. 2018. "Plant Functional Trait Change Across a Warming Tundra Biome." *Nature* 562, no. 7725: 57–62.

Bond-Lamberty, B., A. G. Bunn, and A. M. Thomson. 2012. "Multi-Year Lags Between Forest Browning and Soil Respiration at High Northern Latitudes." *PLoS One* 7, no. 11: e50441.

Bond-Lamberty, B., C. Wang, and S. T. Gower. 2004. "A Global Relationship Between the Heterotrophic and Autotrophic Components of Soil Respiration?" *Global Change Biology* 10: 1756–1766.

Broadbent, A. A., L. K. Newbold, W. J. Pritchard, et al. 2024. "Climate Change Disrupts the Seasonal Coupling of Plant and Soil Microbial Nutrient Cycling in an Alpine Ecosystem." *Global Change Biology* 30, no. 3: e17245.

Broadbent, A. A., H. S. Snell, A. Michas, et al. 2021. "Climate Change Alters Temporal Dynamics of Alpine Soil Microbial Functioning and Biogeochemical Cycling via Earlier Snowmelt." *ISME Journal* 15, no. 8: 2264–2275.

Chen, H., P. Ju, Q. Zhu, et al. 2022. "Carbon and Nitrogen Cycling on the Qinghai-Tibetan Plateau." *Nature Reviews Earth & Environment* 3, no. 10: 701–716.

Choler, P., A. Bayle, B. Z. Carlson, et al. 2021. "The Tempo of Greening in the European Alps: Spatial Variations on a Common Theme." *Global Change Biology* 27, no. 21: 5614–5628.

Choler, P., A. Bayle, N. Fort, and S. Gascoin. 2025. "Waning Snowfields Have Transformed Into Hotspots of Greening Within the Alpine Zone." *Nature Climate Change* 15, no. 1: 80–85.

Ciais, P., C. Sabine, G. Bala, et al. 2014. "Carbon and Other Biogeochemical Cycles." In *Climate Change 2013: The Physical Science Basis. Contribution of Working Group I to the Fifth Assessment Report of the Intergovernmental Panel on Climate Change*, 465–570. Cambridge University Press.

Descombes, P., C. Pitteloud, G. Glauser, et al. 2020. "Novel Trophic Interactions Under Climate Change Promote Alpine Plant Coexistence." *Science* 370, no. 6523: 1469–1473.

Donhauser, J., and B. Frey. 2018. "Alpine Soil Microbial Ecology in a Changing World." *FEMS Microbiology Ecology* 94, no. 9: fiy099.

Edwards, A. C., R. Scalenghe, and M. Freppaz. 2007. "Changes in the Seasonal Snow Cover of Alpine Regions and Its Effect on Soil Processes: A Review." *Quaternary International* 162: 172–181.

Erickson, T. A., M. W. Williams, and A. Winstral. 2005. "Persistence of Topographic Controls on the Spatial Distribution of Snow in Rugged Mountain Terrain, Colorado, United States." *Water Resources Research* 41, no. 4: W04014.

Ernakovich, J. G., K. A. Hopping, A. B. Berdanier, et al. 2014. "Predicted Responses of Arctic and Alpine Ecosystems to Altered Seasonality Under Climate Change." *Global Change Biology* 20, no. 10: 3256–3269.

Fox, J., and S. Weisberg. 2019. *An R Companion to Applied Regression, Third Edition*. Sage.

Freppaz, M., B. L. Williams, A. C. Edwards, R. Scalenghe and E. Zanini, et al. 2007. "Simulating Soil Freeze/Thaw Cycles Typical of Winter Alpine Conditions: Implications for N and P Availability." *Applied Soil Ecology* 35, no. 1: 247–255.

Fu, Z., P. Ciais, I. C. Prentice, et al. 2022. "Atmospheric Dryness Reduces Photosynthesis Along a Large Range of Soil Water Deficits." *Nature Communications* 13, no. 1: 989.

Giardina, C. P., C. M. Litton, S. E. Crow, and G. P. Asner. 2014. "Warming-Related Increases in Soil CO_2 Efflux Are Explained by Increased Below-Ground Carbon Flux." *Nature Climate Change* 4, no. 9: 822–827.

Gitelson, A. A., S. B. Verma, A. Vina, et al. 2003. "Novel Technique for Remote Estimation of CO_2 Flux in Maize." *Geophysical Research Letters* 30, no. 9: 16543.

Hall, D. K., V. V. Salomonson, and G. A. Riggs. 2016. "MODIS/Terra Snow Cover Daily L3 Global 500m Grid – Version 6." NASA National Snow and Ice Data Center – Distributed Active Archive Center.

Happonen, K., A. M. Virkkala, J. Kemppinen, P. Niittynen, and M. Luoto. 2022. "Relationships Between Above-Ground Plant Traits and Carbon Cycling in Tundra Plant Communities." *Journal of Ecology* 110, no. 3: 700–716.

Hicks Pries, C. E., R. S. Van Logtestijn, E. A. Schuur, et al. 2015. "Decadal Warming Causes a Consistent and Persistent Shift From Heterotrophic to Autotrophic Respiration in Contrasting Permafrost Ecosystems." *Global Change Biology* 21: 4508–4519.

Hijmans, R. J. 2022. "*raster: Geographic Data Analysis and Modeling* (R Package Version 3.6–11)."

Hock, R., G. Rasul, C. Adler, et al. 2019. "High Mountain Areas." In *IPCC Special Report on the Ocean and Cryosphere in a Changing Climate*, edited by H.-O. Pörtner, D. C. Roberts, V. Masson-Delmotte, et al., 131–202.

Huete, A., K. Didan, T. Miura, et al. 2002. "Overview of the Radiometric and Biophysical Performance of the MODIS Vegetation Indices." *Remote Sensing of Environment* 83, no. 1–2: 195–213.

Hugonnet, R., R. McNabb, E. Berthier, et al. 2021. "Accelerated Global Glacier Mass Loss in the Early Twenty-First Century." *Nature* 592: 726–731.

Janssens, I. A., H. Lankreijer, G. Matteucci, et al. 2001. "Productivity Overshadows Temperature in Determining Soil and Ecosystem Respiration Across European Forests." *Global Change Biology* 7: 269–278.

Jian, J., V. Bailey, K. Dorheim, et al. 2022. "Historically Inconsistent Productivity and Respiration Fluxes in the Global Terrestrial Carbon Cycle." *Nature Communications* 13, no. 1: 1733.

Jiang, J., Y. Zhang, Y. Wu, et al. 2017. "Relationships Between Aboveground Biomass and Plant Cover at Two Spatial Scales and Their Determinants in Northern Tibetan Grasslands." *Ecology and Evolution* 7, no. 19: 7954–7964.

Jombart, T., S. Devillard, and F. Balloux. 2010. "Discriminant Analysis of Principal Components: A New Method for the Analysis of Genetically Structured Populations." *BMC Genetics* 11: 1–15.

Karnieli, A., N. Ohana-Levi, M. Silver, et al. 2019. "Spatial and Seasonal Patterns in Vegetation Growth-Limiting Factors Over Europe." *Remote Sensing* 11, no. 20: 2406.

Körner, C. 2004. "Mountain Biodiversity, Its Causes and Function." *Ambio* 33, no. sp13: 11–17.

Körner, C. 2021. *Alpine Plant Life: Functional Plant Ecology of High Mountain Ecosystems*. Springer.

Kuzyakov, Y., and O. Gavrichkova. 2010. "Time Lag Between Photosynthesis and Carbon Dioxide Efflux From Soil: A Review of Mechanisms and Controls." *Global Change Biology* 16, no. 12: 3386–3406.

Lefcheck, J. S. 2016. "piecewiseSEM: Piecewise Structural Equation Modelling in R for Ecology, Evolution, and Systematics." *Methods in Ecology and Evolution* 7: 573–579.

Lenoir, J., J. C. Gégout, P. A. Marquet, P. de Ruffray, and H. Brisse. 2008. "A Significant Upward Shift in Plant Species Optimum Elevation During the 20th Century." *Science* 320, no. 5884: 1768–1771.

Lenzi, S., M. Magnani, and I. Baneschi, et al. 2023. "Spatial and Temporal Variability of Carbon Dioxide Fluxes in the Alpine Critical Zone: The Case of the Nivolet Plain, Gran Paradiso National Park, Italy." *PLoS One* 18, no. 5: e0286268.

Liu, H., Z. Mi, L. Lin, et al. 2018. "Shifting Plant Species Composition in Response to Climate Change Stabilizes Grassland Primary Production." *Proceedings of the National Academy of Sciences of the United States of America* 115, no. 16: 4051–4056.

Lyu, Z., P. Sommers, S. K. Schmidt, et al. 2024. "Seasonal Dynamics of Arctic Soils: Capturing Year-Round Processes in Measurements and Soil Biogeochemical Models." *Earth-Science Reviews* 254: 104820.

Macander, M. J., C. S. Swingley, K. Joly, and M. K. Raynolds. 2015. "Landsat-Based Snow Persistence Map for Northwest Alaska." *Remote Sensing of Environment* 163: 23–31.

Maes, S. L., J. Dietricht, G. Midolo, et al. 2024. "Environmental Drivers of Increased Ecosystem Respiration in a Warming Tundra." *Nature* 629: 105–113.

Magnani, M., I. Baneschi, M. Giamberini, et al. 2020. "Drivers of Carbon Fluxes in Alpine Tundra: A Comparison of Three Empirical Model Approaches." *Science of the Total Environment* 732: 139139.

Mainetti, A., S. Ravetto Enri, M. Pittarello, G. Lombardi, and M. Lonati. 2023. "Main Ecological and Environmental Factors Affecting Forage Yield and Quality in Alpine Summer Pastures (NW-Italy, Gran Paradiso National Park)." *Grass and Forage Science* 78, no. 2: 254–267.

Marta, S., A. Zimmer, M. Caccianiga, et al. 2023. "Heterogeneous Changes of Soil Microclimate in High Mountains and Glacier Forelands." *Nature Communications* 14, no. 1: 5306.

Meng, F., A. J. Felton, J. Mao, et al. 2024. "Consistent Time Allocation Fraction to Vegetation Green-Up Versus Senescence Across Northern Ecosystems Despite Recent Climate Change." *Science Advances* 10, no. 23: eadn2487.

Möhl, P., R. S. von Büren, and E. Hiltbrunner. 2022. "Growth of Alpine Grassland Will Start and Stop Earlier Under Climate Warming." *Nature Communications* 13: 7398.

Myers-Smith, I. H., J. T. Kerby, G. K. Phoenix, et al. 2020. "Complexity Revealed in the Greening of the Arctic." *Nature Climate Change* 10, no. 2: 106–117.

Myneni, R. B., and D. L. Williams. 1994. "On the Relationship Between FAPAR and NDVI." *Remote Sensing of Environment* 49, no. 3: 200–211.

Niittynen, P., R. K. Heikkinen, and M. Luoto. 2020. "Decreasing Snow Cover Alters Functional Composition and Diversity of Arctic Tundra." *Proceedings of the National Academy of Sciences of the United States of America* 117: 21480–21487.

Niittynen, P., and M. Luoto. 2018. "The Importance of Snow in Species Distribution Models of Arctic Vegetation." *Ecography* 41, no. 6: 1024–1037.

Parisi, A., F. Avogadro di Valdengo, I. Baneschi, et al. 2024. "Carbon Dioxide Fluxes in Alpine Grasslands at the Nivolet Plain, Gran Paradiso National Park, Italy 2017-2023." *Scientific Data* 11, no. 1: 652.

Pepin, N., E. Arnone, A. Gobiet, et al. 2022. "Climate Changes and Their Elevational Patterns in the Mountains of the World." *Reviews of Geophysics* 60, no. 1: e2020RG000730.

Pepin, N., R. S. Bradley, H. F. Diaz, et al. 2015. "Elevation-Dependent Warming in Mountain Regions of the World." *Nature Climate Change* 5.5: 424–430.

Pinheiro, J. C., and D. M. Bates. 2000. *Mixed-Effects Models in S and S-PLUS*. Springer.

Rounce, D. R., R. Hock, F. Maussion, et al. 2023. "Global Glacier Change in the 21st Century: Every Increase in Temperature Matters." *Science* 379: 78–83.

Rumpf, S. B., M. Gravey, O. Brönnimann, et al. 2022. "From White to Green: Snow Cover Loss and Increased Vegetation Productivity in the European Alps." *Science* 376: 1119–1122.

Schmeller, D. S., J. M. Thornton, D. Urbach, et al. 2024. "Toward a Set of Essential Biodiversity Variables for Assessing Change in Mountains Globally." *Bioscience* 74: biae052.

Sellers, P. J. 1985. "Canopy Reflectance, Photosynthesis and Transpiration." *International Journal of Remote Sensing* 6, no. 8: 1335–1372.

Sistla, S. A., J. C. Moore, R. T. Simpson, et al. 2013. "Long-Term Warming Restructures Arctic Tundra Without Changing Net Soil Carbon Storage." *Nature* 497, no. 7451: 615–618.

Tarquini, S., I. Isola, M. Favalli, et al. 2007. "TINITALY/01: A New Triangular Irregular Network of Italy." *Annales Geophysicae* 50, no. 3: 407–425.

Tarquini, S., I. Isola, M. Favalli, A. Battistini, and G. Dotta. 2023. "TINITALY, a Digital Elevation Model of Italy With a 10 Meters Cell Size (Version 1.1)." Istituto Nazionale di Geofisica e Vulcanologia (INGV), 10.

Theobald, D. M., D. Harrison-Atlas, W. B. Monahan, and C. M. Albano. 2015. "Ecologically-Relevant Maps of Landforms and Physiographic Diversity for Climate Adaptation Planning." *PLoS One* 10, no. 12: e0143619.

Thuiller, W., B. Lafourcade, R. Engler, and M. B. Araújo. 2009. "BIOMOD—A Platform for Ensemble Forecasting of Species Distributions." *Ecography* 32: 369–373.

Tucker, C. J. 1979. "Red and Photographic Infrared Linear Combinations for Monitoring Vegetation." *Remote Sensing of Environment* 8: 127–150.

Viglietti, D., M. Freppaz, G. Filippa, and E. Zanini. 2014. "Soil C and N Response to Changes in Winter Precipitation in a Subalpine Forest Ecosystem, NW Italy." *Hydrological Processes* 28, no. 21: 5309–5321.

Vitasse, Y., S. Ursenbacher, G. Klein, et al. 2021. "Phenological and Elevational Shifts of Plants, Animals and Fungi Under Climate Change in the European Alps." *Biological Reviews* 96: 1816–1835.

Vivaldo, G., M. Magnani, I. Baneschi, et al. 2023. "Carbon Dioxide Exchanges in an Alpine Tundra Ecosystem (Gran Paradiso National Park, Italy): A Comparison of Results From Different Measurement and Modelling Approaches." *Atmospheric Environment* 305: 119758.

Walker, M. D., P. J. Webber, E. H. Arnold, and D. Ebert-May. 1994. "Effects of Interannual Climate Variation on Aboveground Phytomass in Alpine Vegetation." *Ecology* 75, no. 2: 393–408.

Wang, Y., J. Xiao, Y. Ma, et al. 2023. "Persistent and Enhanced Carbon Sequestration Capacity of Alpine Grasslands on Earth's Third Pole." *Science Advances* 9, no. 20: eade6875.

Ward, A., P. Dargusch, S. Thomas, Y. Liu, and E. A. Fulton. 2014. "A Global Estimate of Carbon Stored in the World's Mountain Grasslands and Shrublands, and the Implications for Climate Policy." *Global Environmental Change* 28: 14–24.

Waring, R. H., J. J. Landsberg, and M. Williams. 1998. "Net Primary Production of Forests: A Constant Fraction of Gross Primary Production?" *Tree Physiology* 18: 129–134.

Windmaißer, S., and C. Reisch. 2013. "Long-Term Study of an Alpine Grassland: Local Constancy in Times of Global Change." *Alpine Botany* 123: 1–6.

Winkler, D. E., K. J. Chapin, and L. M. Kueppers. 2016. "Soil Moisture Mediates Alpine Life Form and Community Productivity Responses to Warming." *Ecology* 97, no. 6: 1553–1563.

Xiao, J., Q. Zhuang, D. D. Baldocchi, et al. 2008. "Estimation of Net Ecosystem Carbon Exchange for the Conterminous United States by Combining MODIS and AmeriFlux Data." *Agricultural and Forest Meteorology* 148, no. 11: 1827–1847.

Xu, Z., and G. Zhou. 2011. "Responses of Photosynthetic Capacity to Soil Moisture Gradient in Perennial Rhizome Grass and Perennial Bunchgrass." *BMC Plant Biology* 11: 1–11.

Zemp, M., H. Frey, I. Gärtner-Roer, et al. 2015. "Historically Unprecedented Global Glacier Decline in the Early 21st Century." *Journal of Glaciology* 61, no. 228: 745–762.

Zeng, Y., D. Hao, A. Huete, et al. 2022. "Optical Vegetation Indices for Monitoring Terrestrial Ecosystems Globally." *Nature Reviews Earth & Environment* 3, no. 7: 477–493.

Zhou, S., Y. Zhang, A. P. Williams, and P. Gentine. 2019. "Projected Increases in Intensity, Frequency, and Terrestrial Carbon Costs of Compound Drought and Aridity Events." *Science Advances* 5, no. 1: eaau5740.

Supporting Information

Additional supporting information can be found online in the Supporting Information section. **Text S1:** Model specification for the piecewise SEMs. For each vegetation index, GDD_0 was transformed using the shape parameters estimated for that index, thus VI and βGDD_0 must be considered general notations, and in fact differ among models. Model notation as from piecewise SEM standards. **Figure S1:** (a) Discriminant analysis of principal components based on percent cover of the various plant species groups at the seasonal peak cover. Ellipses represent 1 SD. Violin plots show the distribution of the scores along the main two linear discriminants (LDs) within each sampling site; (b) LD2 and (c) LD1. Black dots mark the median value for each series, while black lines the first and third quartiles. (d) Bar plot reporting the relative contribution (eigenvalues) of the first 4 discriminants; grey bars identify the retained LDs, accounting for 90.90% of the total among-group variance. bare = bare soil + mosses + lichens, forbsL = legumes, forbsO = other forbs, gramiM = medium-leaved graminoids, gramiN = narrow-leaved graminoids, biomD = dry biomass and biomG = green biomass. The different colours represent the different

sampling sites as identified in the legend. **Figure S2:** Temporal distribution of snowmelt dates (a) and seasonal trends for the endogenous variables included in the piecewise SEM (b–h). CO_2 fluxes: (b) gross primary productivity (|*GPP*|) and (c) ecosystem respiration (*ER*). Vegetation indices: (d) *CIred-edge*, (e) *NDVI* and (f) *NIRv*. Instantaneous variables (i.e., environmental variables measured simultaneously with CO_2 fluxes): (g) soil moisture (*soilVWC*) and (h) air temperature (*airT*). The larger scatter for *soilVWC* and *airT* possibly reflects the temporally shorter scale of variation of physical variables, when compared to vegetation (i.e., daily or sub-daily vs. seasonal changes, respectively). Coloured points represent the average value for each sampling occasion (site × date), with bars showing 1 SD around the mean. The different colours represent the different sampling sites as identified in the legend. Background, greyish points represent individual measurements. **Figure S3:** Relationships between environmental predictors and air temperature (*airT*). Effect of (a) irradiance (*swrad*), and (b) multiscale topographic position index (*mTPI*). We show conditional regression plots; shaded areas represent the 95% confidence interval of the average estimates; points are partial residuals. Only statistically significant relationships are reported; standardized coefficients as from piecewise SEMs (Table S3). **Figure S4:** Relationships between environmental predictors and soil moisture (*soilVWC*). Effect of (a) mean summer precipitation ($meanP_s$), and (b) cumulative winter precipitation ($cumP_w$) at different levels of multiscale topographic position index (*mTPI*); effects of (c) cumulated heat (GDD_0) and air temperature (*airT*). We show conditional regression plots; shaded areas represent the 95% confidence interval of the average estimates; points are partial residuals. Interactions were plotted using overlaying cross-sectional plots. The relationships between the response and a continuous predictor are thus shown for three classes of the other predictor (minimum—low, mean—medium and maximum—high values). Only relationships with at least one statistically significant term are reported; standardized coefficients as from piecewise SEMs (Table S3). **Figure S5:** Relationships between environmental predictors and vegetation indices (*CIred-edge*). Effects of Beta-transformed GDD_0 (βGDD_0) at different levels of (a) cumulative winter precipitation ($cumP_w$), and (b) green biomass and legumes (com_1). We show conditional regression plots; shaded areas represent the 95% confidence interval of the average estimates; points are partial residuals. Interactions were plotted using overlaying cross-sectional plots. The relationships between the response and a continuous predictor are thus shown for three classes of the other predictor (minimum—low, mean—medium and maximum—high values). Only relationships with at least one statistically significant term for at least one vegetation index are reported; standardized coefficients as from piecewise SEMs (Table S3). **Figure S6:** Relationships between environmental predictors and gross primary productivity (|*GPP*|) when implementing the *CIred-edge* vegetation index. Effects of (a) vegetation index (*VI*), (b) irradiance (*swrad*), (c) Beta-transformed GDD_0 (βGDD_0), (d) cumulative winter precipitation ($cumP_w$) and (e) community composition (com_1). We show conditional regression plots; shaded areas represent the 95% confidence interval of the average estimates; points are partial residuals. Only relationships with a statistically significant term for at least one vegetation index are reported; standardized coefficients as from piecewise SEMs (Table S3). **Figure S7:** Relationships between environmental predictors and ecosystem respiration (*ER*) when implementing the *CIred-edge* vegetation index. Effects of (a) vegetation index (*VI*), (b) air temperature (*airT*), (c) soil moisture (*soilVWC*), (d) Beta-transformed GDD_0 (βGDD_0), (e) cumulative winter precipitation ($cumP_w$) and (f) community composition (com_1). We show conditional regression plots; shaded areas represent the 95% confidence interval of the average estimates; points are partial residuals. Only relationships with a statistically significant term for at least one vegetation index are reported; standardized coefficients as from piecewise SEMs (Table S3). **Figure S8:** Comparison of coefficients estimated by SEMs integrating the *CIred-edge* vegetation index (reported in Figure 2—on the *y-axis*) and those estimated by models integrating (a) *NDVI* and (b) *NIRv*. Bars represent the standard error of the estimate, as returned by piecewise SEM. **Figure S9:** Variable contribution to each sub-model in terms of variable importance score (single predictors, measuring the joint contribution to both additive and interactive terms). Subscript in (a–f) indicate the vegetation index integrated within each sub-model. Error bars represent the 95% confidence intervals for the average estimate, obtained with 1000 randomizations for each predictor. **Figure S10:** Comparison of coefficients estimated by SEMs integrating the *CIred-edge* vegetation index and based on linear mixed effect (LMM; single point measurements) and simple linear models (LM; sampling occasion averages). Bars represent the standard error of the estimate, as returned by piecewise SEM. **Table S1:** Per-site percent cover (median, 25% and 75% quantiles—median [25%, 75%]) for each of the plant species groups and biomass estimates (ordinal) at the seasonal peak cover. For each site, N reports the number of individual images analyzed; for each group, minimum and maximum observed values (range: min, max) are reported. *bare* = bare soil + mosses + lichens, *forbsL* = legumes, *forbsO* = other forbs, *gramiM* = medium-leaved graminoids, *gramiN* = narrow-leaved graminoids, *biomD* = dry biomass and *biomG* = green biomass. **Table S2:** Variables integrated in structural equation models (piecewise SEMs); variable codes used throughout the text, full explanation with measurement units and source are reported, together with the main spatial and temporal scales of variation. **Table S3:** Standardized coefficients for the piecewise SEM reported in Figure 2, as well as for the models integrating alternative vegetation indices (i.e., *NDVI* and *NIRv*). For each vegetation index, GDD_0 was transformed using the shape parameters estimated for that index, thus *VI* and βGDD_0 must be considered general notations in the table, and in fact differ among models. Significance codes: $0 \leq$ *** ≤ 0.001; $0.001 <$ ** ≤ 0.01; $0.01 <$ * ≤ 0.05.